Variations of ferroelectric off-centering distortion and 3*d*-4*p* orbital mixing in La-doped $BiFeO_3$ multiferroics

Jung-Hoon Lee,[1] Hyoung Joon Choi,[2] Dongeun Lee,[1] Min G. Kim,[3] Chung W. Bark,[1] Sangwoo Ryu,[1] Min-Ae Oak,[1] and Hyun Myung Jang[1,4,*]

[1]*Department of Materials Science and Engineering, and Division of Advanced Materials Science, Pohang University of Science and Technology (POSTECH), Pohang 790-784, Republic of Korea*

[2]*Department of Physics and IPAP, Yonsei University, Seoul 120-749, Republic of Korea*

[3]*Pohang Accelerator Laboratory, Pohang University of Science and Technology (POSTECH), Pohang 790-784, Republic of Korea*

[4]*Department of Physics, Pohang University of Science and Technology (POSTECH), Pohang 790-784, Republic of Korea*

(Received 23 April 2010; revised manuscript received 28 June 2010; published 16 July 2010)

The lanthanum (La) modification is known to improve dielectric and magnetic properties of $BiFeO_3$ (BFO), a promising room-temperature multiferroic oxide. The effects of La doping on the variations of the off-centering distortion and the orbital mixing of BFO are experimentally studied, in conjunction with first-principles density-functional theory (DFT) calculations. Both the Fe-O bond anisotropy in the FeO_6-octahedron cage and the off-centering ferroelectric polarization along the hexagonal $[001]_h$ are predicted to be substantially reduced by the La doping. These DFT predictions agree with the structural-refinement results obtained from high-resolution x-ray powder-diffraction data. We have shown that the apparent improvement of the polarization-field response is not intrinsic and can be attributed to the reduced leakage current by the La doping. X-ray absorption near-edge structure (XANES) spectroscopy study further indicates that the degree of Fe 3*d*-4*p* orbital mixing decreases with the La doping. The conclusion deduced from XANES study correlates well with the orbital-resolved density of states which predicts that the La doping increases the number of unoccupied states in the *p* orbital but suppresses the number of unoccupied states in the Fe 3*d* orbital.

DOI: 10.1103/PhysRevB.82.045113 PACS number(s): 71.15.−m, 77.84.−s, 75.50.Dd

I. INTRODUCTION

Multiferroics are an interesting group of materials that exhibit both ferroelectricity and ferromagnetism with coupled electric and magnetic order parameters.[1] Multiferroism is currently the subject of intensive scientific investigation[2–10] as they potentially offer a wide range of interesting applications.[1,3,6,8] $BiFeO_3$ (BFO) is currently known to be the only ABO_3-type simple perovskite that exhibits room-temperature multiferroism and, thus, is considered to be the most promising candidate for practical applications of multiferroics.[3,11,12] It is a rhombohedrally distorted ferroelectric perovskite ($T_c \approx 1100$ K) with the space group *R*3*c* and shows G-type antiferromagnetism up to 643 K (Néel temperature, T_N).[13–15] The recent boom in multiferroic thin films was indeed triggered by the work of Wang *et al.*[3] on the enhancement of remanent polarization (P_r) and saturation magnetization (M_s) in the epitaxially constrained BFO heterostructures. A more recent study revealed that the enhanced value of M_s in an epitaxially constrained film was proportional to the magnitude of the epitaxial misfit strain and was closely related to the reduced degree of hybridization between Fe 3*d* and O 2*p* orbitals.[16] However, BFO suffers from its high-leakage current (low-electrical resistivity) problem[17–19] coupled with relatively weak tendency of the magnetoelectric (ME) coupling.[20,21]

Numerous attempts were made to reduce the electrical leakage thus to improve the ME coupling characteristics of BFO. Among these, the nonaliovalent lanthanum (La) doping is the most prevalent approach.[22–33] The effect of La doping on the magnetic property of BFO-based ceramics has been investigated rather extensively. The observed enhanced magnetization by the La doping was attributed either to the enhanced ME interaction arising from the destruction of a cycloidal spin structure in the rhombohedral *R*3*c* BFO[19,30] or to a spatial homogenization of the spin arrangement.[24,25] Contrary to this, the study of the La-doping effect on the electrical leakage and ferroelectric property is rare. According to the study done by Zhang and co-workers,[19] the La doping (up to 10 at. %) enhances the apparent value of the ferroelectric switching polarization ($2P_r$) in the polarization-electric field (*P*-*E*) hysteresis curve. In the *P*-*E* measurement, however, they employed increasing values of the maximum applied electric field (E_{max}) from 155 kV/cm for the undoped (pure) BFO to 305 kV/cm for the 20 at. % La-doped BFO (i.e., $Bi_{1-x}La_xFeO_3$ with $x=0.20$) polycrystalline ceramic. When they used the same value of E_{max} at 200 kV/cm, the La doping even decreased the value of $2P_r$ up to $x=0.20$. However, they did not report the La-doing effect on the electrical leakage characteristics of BFO-based ferroics.

At the present stage, thus, it is not clear whether the apparent change in P_r truly reflects the variation of the off-centering ferroelectric distortion or is simply related to a reduced electrical leakage by the La doping. In view of this uncertainty, one of main purposes of the present study is to clarify the effect of La doping on the degree of the ferroelectric off-centering distortion, in conjunction with the variation of the Fe-O bond anisotropy at the FeO_6-octahedron cage which is responsible for manifesting a spin-canted weak ferromagnetism. First-principles density-functional theory (DFT) calculations support our experimental results that the La doping significantly decreases the ferroelectric off-centering distortion as a result of the reduced degree of the Bi-ion displacement along the hexagonal $[001]_h$. The x-ray

absorption near-edge structure (XANES) spectroscopy study interestingly reveals that the degree of the $3d$-$4p$ orbital mixing also decreases with the La doping. We have quantitatively explained this spectroscopic observation using the computed partial density of states (DOS) of Fe p and Fe d orbitals.

II. EXPERIMENTAL AND COMPUTATIONAL DETAILS

Pure and La-doped BFO powder samples used in the present study were prepared by a conventional solid-state-reaction method. Stoichiometric amounts of high-purity Bi_2O_3 (Kojundo Chem. Laboratory. Co., 99.99%), Fe_2O_3 (Kojundo Chem. Laboratory. Co., 99.99%), and La_2O_3 (Sigma-Aldrich, Inc., 99.99%) powders were mixed and ball milled in a high-purity ethanol medium for 24 h. The pure BFO mixture was then calcined at 650 °C for 1 h and subsequently at 810 °C for 1 h, followed by thorough grinding. On the other hand, the La-doped BFO powders ($Bi_{1-x}La_xFeO_3$ with $x=0.08$ and 0.15) were calcined at 800 °C for 10 h to ensure the stoichiometric A-site substitution of La ions for Bi ions. The synthesized powders were then leached with dilute nitric acid and finally the desired powers ($R3c$ rhombohedral symmetry) without having any impurity phase and divalent Fe^{2+} were obtained. For dielectric measurements of polycrystalline ceramic pellets, both calcined BFO and La-doped BFO powders were cold-isostatically-pressed at 200 MPa and subsequently sintered at 830 °C in air for 1 h. Electrical properties (dielectric permittivity, I-V curve, and Cole-Cole plot) of the sintered ceramic pellets were measured using an impedance analyzer (HP 4194).

High-resolution powder-diffraction (HRPD) experiment was done at 8C2 beamline of the Pohang Light Source (PLS) at Pohang Accelerator Laboratory. The incident x-ray was monochromatized to the wavelength of 1.544 Å using a double-bounce Si (111) monochromator. The diffraction patterns were collected over 2θ range of $10°-135°$ with a step size 0.0024° and a counting time of 2 s per step. The crystal structure was determined by comparing the experimentally collected HRPD pattern with the calculated pattern using the Rietveld method (RIETAN-2000). The structural parameters such as lattice parameter and bond distance were refined accurately within the allowed error range. The HRPD data were also refined by utilizing the software called "POWDER CELL program"[34] to cross-check the Rietveld-refined results. Optimization procedures were continued until the difference in the refined result between these two methods is less than 5%. For a possible correlation of the structural change arising from the La doping with the variation of the orbital states, we carefully measured XANES and extended x-ray absorption fine structure (EXAFS) spectra at synchrotron 7C1 XAFS beamline of the PLS. The fluorescence mode was used for the measurement.

To quantitatively understand the effect of La doping on the degree of the atomic distortion and the DOS, we performed first-principles DFT calculations on the basis of the generalized gradient approximation[35] and the GGA+U method[36] implemented with the projector augmented wave[37,38] pseudopotential using the Vienna *ab initio* simulation package.[39,40] The Hubbard U_{eff} of 4.5 eV was chosen on the basis of empirical corrections. We explicitly treated five valence electrons for Bi ($6s^26p^3$), nine for La ($4p^65s^26d^1$), eight for Fe ($3d^64s^2$), and six for oxygen ($2s^22p^4$). All these calculations were performed using (i) a $4\times4\times3$ Monkhorst-Pack k-point mesh[41] centered at Γ for $R3c$ structure, (ii) a 500 eV plane-wave cutoff, and (iii) the tetrahedron method with the Blöchl corrections for the Brillouin-zone integrations.[42] The structural optimizations were performed for the 30-atoms cell which corresponds to a hexagonal unit cell. The ions were relaxed until the forces on them were less than 0.01 eV/Å. The off-centering ferroelectric polarization was calculated by exploiting the Berry-phase method of Vanderbilt and King-Smith.[43,44] We performed DFT computations for two compositions: (i) undoped BFO and (ii) one La ion substituted for one Bi ion per hexagonal unit cell (i.e., per six BFO formula cells). Thus, the latter corresponds to 17 ($\approx100/6$) at. % La doping in $R3c$ BFO.

III. RESULTS AND DISCUSSION

A. Refined crystal structure and electron localization function

Figure 1(a) presents high-resolution synchrotron x-ray diffraction (HR-XRD) patterns of pure (undoped) and La-doped BFO powders at three different compositions, namely, $Bi_{1-x}La_xFeO_3$ with $x=0$, 0.08, and 0.15. The three HR-XRD patterns indicate that both BFO and La-doped BFO powders do not contain any impurity phase. All three patterns at room temperature agree well with the standard Joint Committee for Powder Diffraction Standard diffraction pattern of the rhombohedral $R3c$ symmetry. The HR-XRD data were carefully refined to obtain information on the variation of local atomic structure by the La substitution. Figure 1(b) presents the Rietveld refinement result of the pure BFO powder as an example. The following values were obtained for the three representative reliability factors (R): $R_p=1.95$, $R_{wp}=2.57$, and $R_{\exp}=1.59$. These values ensure the reliability of the present Rietveld refinement. The refined lattice parameters of the hexagonal unit cell for three different $Bi_{1-x}La_xFeO_3$ powders are (i) $a=5.57987$ Å, $c=13.87229$ Å for $x=0$ (i.e., pure BFO), (ii) $a=5.57976$ Å, $c=13.86375$ Å for $x=0.08$, and (iii) $a=5.57923$ Å, $c=13.85279$ Å for $x=0.15$.

Figure 2(a) presents a schematic drawing of the refined crystal structure of the hexagonal unit cell of the undoped BFO containing six $BiFeO_3$ formula cells (i.e., 30 atoms), showing six corner-sharing FeO_6-octahedron units per hexagonal cell. Figure 2(a) also shows two distinct kinds of the nearest-neighbor Fe-O bonds (Fe-O1 and Fe-O2) in the FeO_6-octahedron cage. As presented in Fig. 2(b), the three oxygen ions located at the upper half plane (along the c axis) of the FeO_6 cage belong to "O1." On the other hand, the three remaining oxygen ions at the lower half plane of the FeO_6 cage belong to "O2." Figure 2(b) also shows that the Bi ion at the A site is displaced from its centrosymmetric position. According to our DFT calculations, the off-centering Bi-ion displacement along the c xis of the undoped BFO is ~0.39 Å [=(3.879−3.094)/2 Å]. On the other hand, the off-centering distortion of the Fe ion at the FeO_6-octahedron

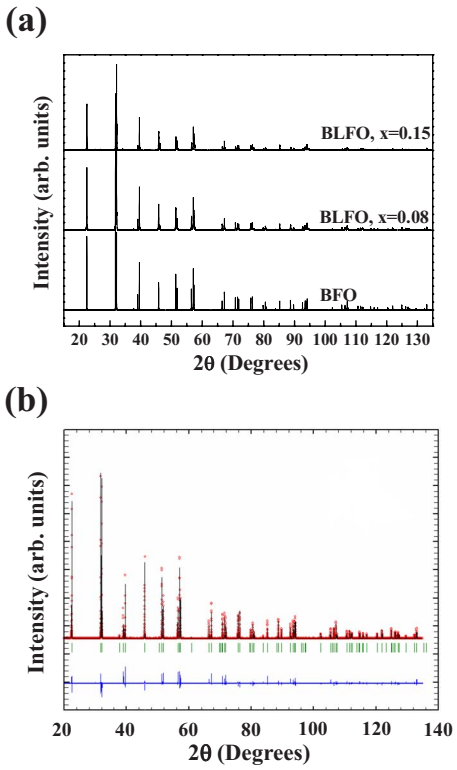

FIG. 1. (Color online) (a) Room-temperature HR-XRD patterns of BFO-based powders at three different compositions, namely, $Bi_{1-x}La_xFeO_3$ with x=0, 0.08, and 0.15. (b) An example of the Rietveld refinement using the diffraction pattern of the undoped BFO. In the pattern, the red-colored points represent the measured intensity at different 2θ values while the black-colored lines denote the refined profile. The Bragg reflection positions are marked with the green-colored vertical lines and the difference profile is shown by the blue-colored lines at the bottom.

cage is relatively negligible. These DFT results agree well with the refined results (both Rietveld analysis and POWDER CELL program[34]). According to the previous DFT studies,[21,33,45,46] the stereochemically active lone-pair electrons originating from the hybridization of 6*s* and 6*p* atomic orbitals of Bi are responsible for the off-centering displacement of the Bi ion along the *c* axis of the hexagonal cell or, equivalently, along $[111]_c$ of the pseudocubic unit cell.

The electron localization function (ELF) is an informative tool to distinguish different bonding interactions in solids.[47] As shown in the left-hand-side contour of Fig. 2(c), negligibly small values of the computed ELF between atoms indicate a dominant ionic bonding character for both Fe-O and Bi-O, and this conclusion agrees with the previous DFT result reported by Ravindran *et al.*[46] According to the ELF result of the pure BFO, the electron density is maximum at the O sites and is minimum at the Fe site. This clearly demonstrates a metal-to-ligand charge transfer process in the *R*3*c* BFO. In addition, Fig. 2(c) shows the off-centering displacement of Bi along $[001]_h$ (i.e., or along $[111]_c$).

As shown in the right-hand-side contour, the La-ion substitution alters a local structure greatly. It is interesting to notice that the Fe ion in the octahedron cage now moves to a more symmetric position. Consequently, the Fe-O bond an-

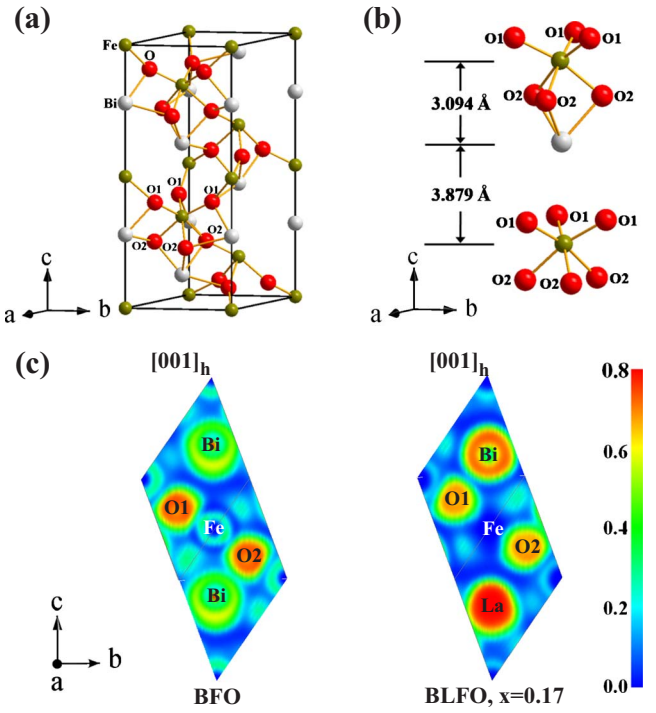

FIG. 2. (Color online) (a) A schematic drawing of the refined hexagonal unit-cell structure of BFO containing six $BiFeO_3$ formula cells (30 atoms). The refined structure shows (i) six corner-sharing FeO_6-octahedron units per hexagonal cell and (ii) two distinct kinds of the nearest-neighbor Fe-O bonds (Fe-O1 and Fe-O2) in the FeO_6-octahedron cage. (b) A local atomic structure centered at the *A*-site Bi ion of an ABO_3-type perovskite lattice, showing the off-centering displacement of the Bi ion along the *c* axis of the hexagonal cell. According to the DFT calculations this off-centering distortion in the undoped BFO is predicted to be ~0.39 Å which nearly coincides with the Rietveld refinement result. Notice that due to the off-centering distortion along the *c* axis, the Bi-O1 bond distance is significantly longer than the Bi-O2 bond distance. (c) The computed ELF plotted along the *c* axis of the hexagonal unit cell. The ELF contours were obtained by performing DFT calculations of the rhombohedral *R*3*c* unit cell containing ten atoms. The left-hand-side contour presents the ELF plot of the pure BFO whereas the right-hand-side contour shows the ELF plot of the 17 at. % La-modified BFO.

isotropy (e.g., the difference in the bond distance between Fe-O1 and Fe-O2) reduces significantly upon the substitution of La ion for Bi ion at the *A* site of perovskite lattice. The La-ion substitution not only alters a local structure but also induces a variation in the electron density. As shown in Fig. 2(c), the electron density at the Fe core decreases substantially upon the La-ion substitution for Bi. Interestingly, this reduced electron density at the Fe-ion site accompanies with an enhanced electron density at the La core (stronger electronegativity of La ion as compared with that of Bi ion). This suggests that the oxidation state of the Fe ion increases slightly upon the La-ion substitution for Bi.

B. Ferroelectric off-centering distortion and FeO_6-octahedron cage

Figure 3(a) presents the variation of the Fe-O bond distance with the La-doping content. The colored filled circles

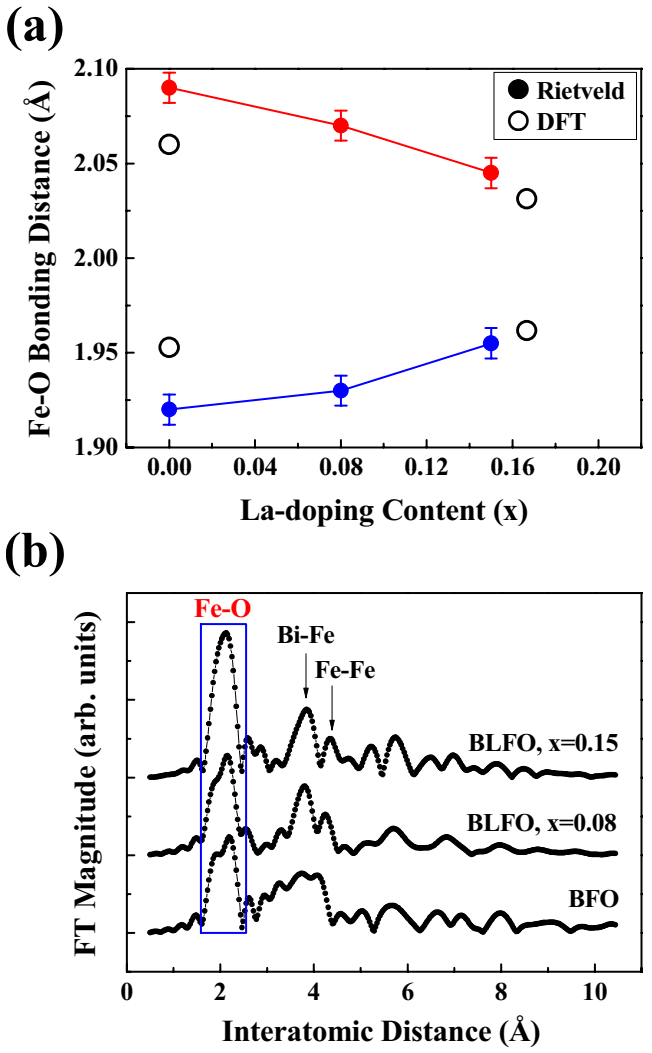

FIG. 3. (Color online) (a) The variation of the Fe-O bond distance with the La doping. The color-filled circles denote the two distinct bond distances (Fe-O1 and Fe-O2) obtained from the Rietveld refinement of HR-XRD patterns whereas the open circles represent the computed DFT values. (b) Room-temperature Fe *K*-edge EXAFS spectra of BFO-based powders at three different compositions, namely, $Bi_{1-x}La_xFeO_3$ with $x=0$, 0.08, and 0.15.

denote the two distinct bond distances (Fe-O1 and Fe-O2) obtained from the Rietveld refinement of HR-XRD patterns whereas the open circles represent the computed DFT values. Both the refined results and the DFT calculations predict that the FeO_6-octahedron cage becomes progressively uniform with the La content, which indicates a gradual decrease in the local structural distortion of the FeO_6-octahedron cage with the La doping.[33] We have cross-checked the conclusion deduced from the crystal-structure refinement and the DFT calculations by examining the effect of the La modification on the Fe *K*-edge EXAFS spectrum. The radial distribution function, as obtained by Fourier transform of the EXAFS function, $\chi(k)$, into real space, demonstrates that the two distinct peaks (doublet) corresponding to the first-shell Fe-O bonds gradually merge into a single peak with increasing La-doping content [Fig. 3(b)]. Thus, our conclusion obtained from the structure refinement and the DFT calculations is also supported by hard x-ray absorption spectroscopy analysis.

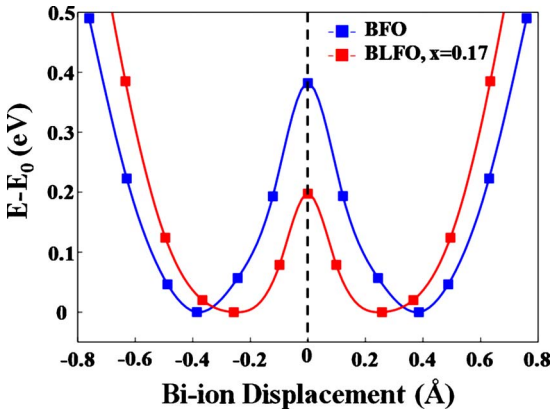

FIG. 4. (Color online) A comparison of the double-well potential of the pure BFO with that of the 17 at. % La-doped BFO. The computed Kohn-Sham energy is plotted as a function of the Bi-ion displacement (from its centrosymmetric position) along the *c* axis of the hexagonal cell.

Though the structurally anisotropic FeO_6-octahedron cage shows an interesting tendency of the Fe-O bond homogeneity with the La doping, its off-centering distortion is negligible as mentioned previously. Both the structure refinement and the DFT calculations indicate that this statement remains valid for La-doped BFOs. On the other hand, we have found that for both pure and La-doped BFOs (up to 17 at. % La substitution), the stereochemically active 6*s* lone pair of Bi is mainly responsible for the off-centering ferroelectric distortion along the *c* axis of the hexagonal cell. However, as presented in Fig. 4, the off-centering displacement of the Bi ion (from the centrosymmetric position) along the *c* axis is significantly reduced by the La doping. Our structure refinement qualitatively agrees with this DFT prediction. The Berry-phase polarization calculations further predict that a large polarization of 86 $\mu C/cm^2$ for the undoped BFO is reduced to 36 $\mu C/cm^2$ by 17 at. % La doping. It is interesting to notice that the La doping substantially reduces the barrier height of the double-well potential, which, in turn, reduces the stability of the off-centering ferroelectricity against thermal agitation (Fig. 4). In view of these DFT results, one can make the statement that the La doping substantially reduces not only the ferroelectric polarization but also the displacive ferroelectric character. Thus, the reported apparent improvement of the *P-E* curve by the La doping[19] is not caused by the enhanced off-centering ferroelectric polarization but originates from some other extrinsic effects.

C. Reduced leakage current by the La doping

As shown in the current-voltage (*I-V*) curves, the La doping substantially reduces the leakage current of BFO-based polycrystalline pellets [Fig. 5(a)]. The Cole-Cole plot presented in Fig. 5(b) also shows that the La doping greatly enhances the resistivity and, thus, supports the result of *I-V* curves. Thus, the apparent improvement of the *P-E* response by the La doping[19] does not reflect the variation of the ferro-

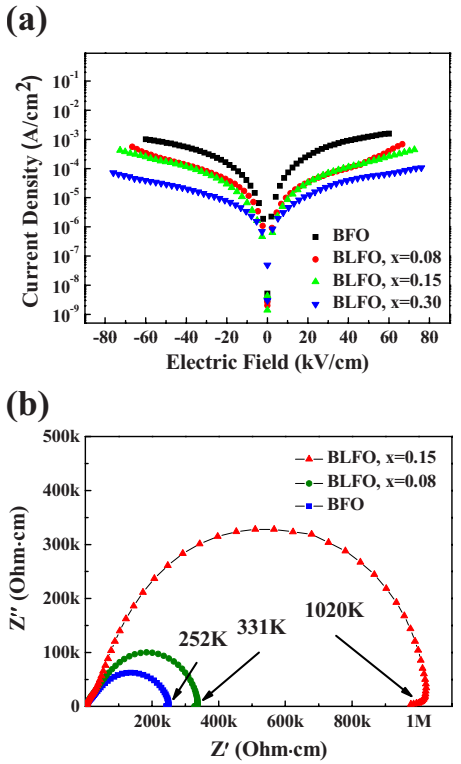

FIG. 5. (Color online) (a) *I-V* curves of BFO-based sintered ceramic pellets at four different compositions, namely, $Bi_{1-x}La_xFeO_3$ with $x=0$, 0.08, 0.15, and 0.30. (b) Complex impedance patterns of BFO-based sintered ceramic pellets at three different La contents, namely, $x=0$, 0.08, and 0.15.

electric off-centering distortion but is simply related to a reduced electrical leakage. By virtue of this enhanced electrical resistivity by the La doping, Zhang and co-workers[19] were able to increase the maximum applied electric field (E_{max}) in their *P-E* measurements: from 155 kV/cm for the undoped BFO to 305 kV/cm for the 20 at. % La-doped BFO. This consequently leads to an increase in the apparent value of $2P_r$ (net switching polarization) with the La doping.

The dielectric permittivity estimated from the peak of a semicircle in the complex impedance spectrum [Fig. 5(b)] indicates that the main semicircle is caused by a conducting mechanism at the bulk grains. This suggests that the observed change in the resistivity by the La doping does not stem from minor amounts of secondary phases at grain boundaries. The synchrotron HR-XRD data also support the absence of any minority phase. Therefore, the apparent improvement of the *P-E* curve by the La doping can be interpreted in terms of the enhanced electrical resistivity in the bulk grains, not at grain boundaries. It has been recently reported that the charge carrier of BFO-based perovskite oxides (e.g., $BiFe_{1-x}Mn_xO_3$) is a hole rather than an electron (*p*-type carrier).[48] According to this proposition, the observed increase in the electrical resistivity (Fig. 5) can be attributed to a reduction in the concentration of minor hole carriers or the fraction of Fe^{4+} ions by the La doping. However, a more systematic study is needed to clearly identify the underlying mechanism of this enhanced resistivity by the La doping.

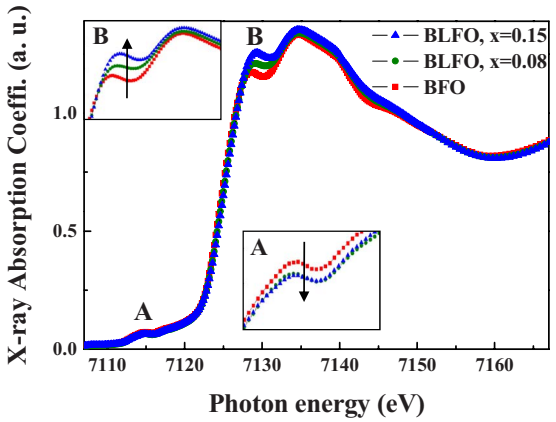

FIG. 6. (Color online) Fe *K*-edge XANES spectra of La-modified BFO ($Bi_{1-x}La_xFeO_3$) powders at three different La contents, namely, $x=0$, 0.08, and 0.15.

D. Fe 3*d*-4*p* orbital mixing

Figure 6 presents the Fe *K*-edge XANES spectra of La-modified BFO ($Bi_{1-x}La_xFeO_3$) powders at three different La contents, namely, $x=0$, 0.08, and 0.15. In Fig. 6, the normalized x-ray absorption coefficient is plotted as a function of photon energy. The pre-edge peak **A** corresponds to the $1s$-$3d$ electric dipole-forbidden transition ($\Delta l=\pm 2$. $\therefore |\langle nlm_l|u|n'l'm_l'\rangle|^2=0$). This weak-intensity peak is known to be a consequence of the Fe $3d$-$4p$ orbital mixing (hybridization).[49] Because of a partially endowed *p*-orbital character by the $3d$-$4p$ hybridization, the intensity of this forbidden peak is not strictly zero (Fig. 6). On the other hand, the peak **B** corresponds to the $1s$-$4p$ electric dipole-allowed transition ($\Delta l=\pm 1$, $\Delta m_l=0,\pm 1$. $\therefore |\langle nlm_l|u|n'l'm_l'\rangle|^2\neq 0$). As shown in the insets of Fig. 6, the intensity of the peak **A** reduces while the intensity of the peak **B** enhances with increasing La content. These converse effects can be explained in terms of the difference in the degree of the $3d$-$4p$ orbital mixing which arises from the variation of local structure by the La doping.

The undoped BFO possesses a highly distorted noncentrosymmetric structure which is characterized by a relatively large off-centering distortion of the Bi ion and by a structural anisotropy in the FeO_6-octahedron cage (Fig. 2). However, the La doping reduces both the off-centering distortion (Fig. 4) and the Fe-O bond anisotropy in the FeO_6-octahedron cage (Fig. 3). Thus, the degree of the $3d$-$4p$ orbital mixing is expected to be more pronounced[49] in the highly distorted undoped BFO ($x=0$). Consequently, the intensity of the peak **A** which originates from the $1s$-$3d$ dipole-forbidden transition reduces progressively as the La content increases because of the reduced degree of the $3d$-$4p$ orbital mixing with the La doping. On the other hand, the intensity of the peak **B** which corresponds to the $1s$-$4p$ dipole-allowed transition enhances with the La doping. Thus, the XANES results are consistent with the previous finding that the La doping reduces both the off-centering displacement and the Fe-O bond anisotropy in the FeO_6-octahedron cage.

E. Orbital-resolved density of states

We have carefully examined the orbital-resolved DOS to understand the XANES spectroscopy results from first prin-

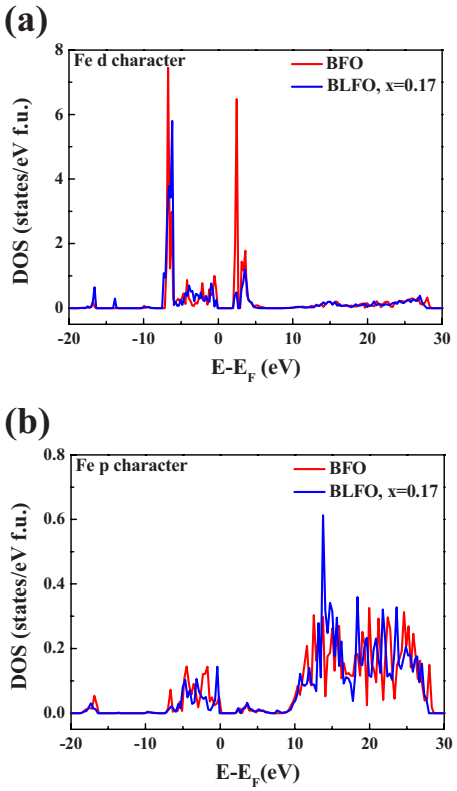

FIG. 7. (Color online) A comparison of the partial DOS of the pure BFO with that of the 17 at. % La-doped BFO. The upper panel (a) presents the computed orbital-resolved DOS for the Fe 3*d* orbital whereas the bottom panel (b) shows the orbital-resolved DOS for the *p* orbitals.

ciples. Because of the reduced degree of the 3*d*-4*p* orbital mixing associated with the reduced structural distortion, the La doping is expected to decrease the number of occupied states in the Fe *p* orbital $(2p,3p)$ but increases the number of occupied states in the Fe *d* orbital $(3d)$. In parallel with these changes in the occupied states, the La doping simultaneously increases the number of unoccupied states in the Fe *p* orbital $(4p)$ but decreases the number of unoccupied states in the Fe *d* orbital. Interestingly, the computed orbital-resolved DOS of the Fe ion presented in Fig. 7 does accord well with these predictions. Table I summarizes these changes in numerical values (states per formula unit).

As shown in Fig. 7, the density of unoccupied states of the Fe 3*d* orbital decreases most prominently at the Kohn-Sham energy of ~2 eV above the Fermi level $[\equiv E_u(d)]$ by

TABLE I. Calculated orbital-dependent occupied and unoccupied states of the Fe atom in the undoped BFO and the 17 at. % La-doped BFO.

		Fe *p* character	Fe *d* character
BFO, $x=0$	Occupied states	1.68	22.61
	Unoccupied states	9.86	14.10
BLFO, $x=0.17$	Occupied states	1.25	27.70
	Unoccupied states	10.34	4.96

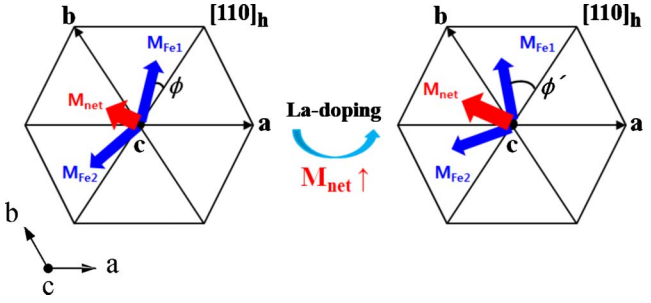

FIG. 8. (Color online) Schematic diagrams showing the effect of La doping on the spin structure and the resulting magnetization vector oriented perpendicular to $[110]_h$.

the La doping. This reduced density of the unoccupied *d* states does correspond to the reduced intensity of the peak **A** which originates from the 1*s*-3*d* dipole-forbidden transition (Fig. 6). On the other hand, the La doping most prominently enhances the density of unoccupied states of the Fe *p* orbital at the Kohn-Sham energy of ~15 eV above the Fermi level $[\equiv E_u(p)]$. In this case, the enhanced density of the unoccupied *p* states does correspond to the enhanced intensity of the peak **B** (arising from the 1*s*-4*p* dipole-allowed transition) by the La doping. According to this interpretation, the energy difference, $E_u(p)-E_u(d)$, should be equal to $E_{peak\ B}-E_{peak\ A}$. Thus, our DFT computations read $E_u(p)-E_u(d)=E_{peak\ B}-E_{peak\ A}=\sim(15-2)$ eV $=\sim 13$ eV. Interestingly, this DFT value nearly coincides with the energy difference deduced from the XANES spectra of Fig. 6, namely, $\sim(7128-7115)$ eV $=\sim 13$ eV. Therefore, the reduced degree of the 3*d*-4*p* orbital mixing by the La doping, which has been deduced from the XANES spectra, directly reflects our DFT prediction that the La doping enhances the number of unoccupied states in the Fe *p* orbital but suppresses the number of unoccupied states in the Fe *d* orbital.

F. Spin canting from $[110]_h$

Finally, we have examined the effect of La doping on the spin anting and the resulting magnetization vector. As schematically shown in Fig. 8, the DFT calculations (taking into account the spin-orbit coupling) predict that for both undoped and La-doped BFOs, the net canted moment is perpendicular to the hexagonal $[110]_h$ direction, irrespective of the doping. Notice that $\mathbf{M}_{Fe1}$ and $\mathbf{M}_{Fe2}$ vectors are projected onto the *a*-*b* basal plane. Thus, they do not lie on the same plane: ferromagnetic coupling on the same basal plane but canted antiferromagnetic (AFM) coupling along the *c* axis. Thus, the ground-state spin configuration of the pure BFO can be approximated by a A-type canted AFM structure.[46] This conclusion is also valid for La-doped BFOs. However, the net canted moment is predicted to be significantly enhanced by the La doping: from 0.11 emu/g for the undoped BFO to 0.21 emu/g for the 17 at. % La-doped BFO.

The enhanced magnetization by the doping accompanies with a small variation of the spin-canting angle from the hexagonal $[110]_h$ direction, as schematically shown in Fig. 8. According to our DFT calculations, the canting angle (ϕ) increases slightly from 0.203° for the undoped BFO to

0.226° for the 17 at. % La-doped BFO, which leads to the increase in the net canted moment on the *a*-*b* plane but leaves the magnetic easy axis unchanged. Thus, the observed enhanced magnetization by the La doping[19,24,25,30] can be attributed, at least partly, to the variation of the spin-canting angle associated with the La doping. Considering the dominant role of the Fe-magnetic moment in the total magnetic moment, one can further correlate the enhanced magnetization with the reduced degree of the 3*d*-4*p* orbital mixing by the La doping, thus, with the increase in the number of occupied states in the Fe 3*d* orbital (Table I).

IV. CONCLUSIONS

The following conclusions are made from the present experimental and computational studies of the La-doping effects on the ferroelectric off-centering distortion and the 3*d*-4*p* orbital mixing of BFO multiferroics with *R*3*c* symmetry. (i) Both the off-centering ferroelectric distortion and the Fe-O bond anisotropy of the FeO_6-octahedron cage decrease with the La doping. (ii) The apparent improvement of the *P*-*E* curve by the La modification is not intrinsic and can be attributed to the reduced leakage current by the La doping. (iii) XANES spectra indicate that the degree of the 3*d*-4*p* orbital mixing decreases with the La doping. (iv) The computed orbital-resolved density of states predicts that the La doping increases the number of unoccupied states in the *p* orbital but decreases the number of unoccupied states in the Fe 3*d* orbital. This is closely related to the reduced degree of the 3*d*-4*p* orbital mixing by the La doping.

ACKNOWLEDGMENTS

All the x-ray spectroscopic and diffraction measurements were carried out at the Pohang Light Source (PLS) of Pohang Accelerator Laboratory, POSTECH. This work was supported by the Korea Research Foundation (KRF) under Contract No. KRF-2008-313-C00252 and by WCU (World Class University) program through the National Research Foundation of Korea funded by the Ministry of Education, Science and Technology (Grant No. R31-2008-000-10059-0).

*Author to whom correspondence should be addressed; hmjang@postech.ac.kr

[1] N. A. Hill, J. Phys. Chem. B **104**, 6694 (2000).
[2] R. Seshadri and N. A. Hill, Chem. Mater. **13**, 2892 (2001).
[3] J. Wang, J. B. Neaton, H. Zheng, V. Nagarajan, S. B. Ogale, B. Liu, D. Viehland, V. Vaithyanathan, D. G. Schlom, U. V. Waghmare, N. A. Spaldin, K. M. Rabe, M. Wuttig, and R. Ramesh, Science **299**, 1719 (2003).
[4] T. Kimura, T. Goto, H. Shintani, K. Ishizaka, T. Arima, and Y. Tokura, Nature (London) **426**, 55 (2003).
[5] N. Hur, S. Park, P. A. Sharma, J. S. Ahn, S. Guha, and S. W. Cheong, Nature (London) **429**, 392 (2004).
[6] T. Lottermoser, T. Lonkai, U. Amann, D. Hohlwein, J. Ihringer, and M. Fiebig, Nature (London) **430**, 541 (2004).
[7] N. Ikeda, H. Ohsumi, K. Ohwada, K. Ishii, T. Inami, K. Kakurai, Y. Murakami, K. Yoshii, S. Mori, Y. Horibe, and H. Kito, Nature (London) **436**, 1136 (2005).
[8] W. Eerenstein, N. D. Mathur, and J. F. Scott, Nature (London) **442**, 759 (2006).
[9] S. M. Selbach, T. Tybell, M.-A. Einarsrud, and T. Grande, Chem. Mater. **19**, 6478 (2007).
[10] S. Ishiwata, Y. Taguchi, H. Murakawa, Y. Onose, and Y. Tokura, Science **319**, 1643 (2008).
[11] G. Catalan and J. F. Scott, Adv. Mater. **21**, 2463 (2009).
[12] S. Ryu, J. Y. Son, Y.-H. Shin, H. M. Jang, and J. F. Scott, Appl. Phys. Lett. **95**, 242902 (2009).
[13] F. Kubel and H. Schmid, Acta Crystallogr., Sect. B: Struct. Sci. **46**, 698 (1990).
[14] P. Fischer, M. Połomska, I. Sosnowska, and M. Szymański, J. Phys. C **13**, 1931 (1980).
[15] B. Ruette, S. Zvyagin, A. P. Pyatakov, A. Bush, J. F. Li, V. I. Belotelov, A. K. Zvezdin, and D. Viehland, Phys. Rev. B **69**, 064114 (2004).
[16] S. Ryu, J.-Y. Kim, Y.-H. Shin, B.-G. Park, J. Y. Son, and H. M. Jang, Chem. Mater. **21**, 5050 (2009).
[17] Y. P. Wang, L. Zhou, M. F. Zhang, X. Y. Chen, J.-M. Liu, and Z. G. Liu, Appl. Phys. Lett. **84**, 1731 (2004).
[18] A. K. Pradhan, K. Zhang, D. Hunter, J. B. Dadson, G. B. Loutts, P. Bhattachara, R. S. Katiyar, J. Zhang, D. J. Sellmyer, U. N. Roy, Y. Cui, and A. Burger, J. Appl. Phys. **97**, 093903 (2005).
[19] S.-T. Zhang, L.-H. Pang, Y. Zhang, M.-H. Lu, and Y.-F. Chen, J. Appl. Phys. **100**, 114108 (2006).
[20] S.-W. Cheong and M. Mostovoy, Nature Mater. **6**, 13 (2007).
[21] J. B. Neaton, C. Ederer, U. V. Waghmare, N. A. Spaldin, and K. M. Rabe, Phys. Rev. B **71**, 014113 (2005).
[22] I. Sosnowska, M. Loewenhaupt, W. I. F. David, and R. M. Ibberson, Mater. Sci. Forum **133-136**, 683 (1993).
[23] Z. V. Gabbasova, M. D. Kuz'min, A. K. Zvezdin, I. S. Dubenko, V. A. Murashov, D. N. Rakov, and I. B. Krynetsky, Phys. Lett. A **158**, 491 (1991).
[24] A. V. Zalesskiĭ, A. A. Frolov, T. A. Khimich, and A. A. Bush, Fiz. Tverd. Tela (Leningrad) **45**, 134 (2003). Phys. Solid State **45**, 141 (2003).
[25] D. Lee, M. G. Kim, S. Ryu, H. M. Jang, and S. G. Lee, Appl. Phys. Lett. **86**, 222903 (2005).
[26] G. L. Yuan, K. Z. Baba-Kishi, J.-M. Liu, S. W. Or, Y. P. Wang, and Z. G. Liu, J. Am. Ceram. Soc. **89**, 3136 (2006).
[27] Y.-P. Liu and J.-M. Wu, Electrochem. Solid-State Lett. **10**, G39 (2007).
[28] G. L. Yuan, S. W. Or, and H. L. W. Chan, J. Phys. D **40**, 1196 (2007).
[29] Y. Yoneda, K. Yoshii, H. Saitoh, and J. Mizuki, Ferroelectrics **348**, 33 (2007).
[30] Y.-H. Lin, Q. Jiang, Y. Wang, C.-W. Nan, L. Chen, and J. Yu, Appl. Phys. Lett. **90**, 172507 (2007).
[31] S. R. Das, R. N. P. Choudhary, P. Bhattacharya, R. S. Katiyar, P. Dutta, A. Manivannan, and M. S. Seehra, J. Appl. Phys. **101**, 034104 (2007).

[32] H. M. Jang, J. H. Park, S. Ryu, and S. R. Shannigrahi, Appl. Phys. Lett. **93**, 252904 (2008).
[33] Z. Zhang, P. Wu, L. Chen, and J. Wang, Appl. Phys. Lett. **96**, 012905 (2010).
[34] W. Kraus and G. J. Nolze, J. Appl. Crystallogr. **29**, 301 (1996).
[35] J. P. Perdew, K. Burke, and Y. Wang, Phys. Rev. B **54**, 16533 (1996).
[36] V. I. Anisimov, F. Aryasetiawan, and A. I. Liechtenstein, J. Phys.: Condens. Matter **9**, 767 (1997).
[37] P. E. Blöchl, Phys. Rev. B **50**, 17953 (1994).
[38] G. Kresse and D. Joubert, Phys. Rev. B **59**, 1758 (1999).
[39] G. Kresse and J. Hafner, Phys. Rev. B **47**, 558 (1993).
[40] G. Kresse and J. Furthmüller, Phys. Rev. B **54**, 11169 (1996).
[41] H. J. Monkhorst and J. D. Pack, Phys. Rev. B **13**, 5188 (1976).
[42] P. E. Blöchl, O. Jepsen, and O. K. Andersen, Phys. Rev. B **49**, 16223 (1994).
[43] R. D. King-Smith and D. Vanderbilt, Phys. Rev. B **47**, 1651 (1993).
[44] D. Vanderbilt and R. D. King-Smith, Phys. Rev. B **48**, 4442 (1993).
[45] C. Ederer and N. A. Spaldin, Phys. Rev. Lett. **95**, 257601 (2005).
[46] P. Ravindran, R. Vidya, A. Kjekshus, H. Fjellvåg, and O. Eriksson, Phys. Rev. B **74**, 224412 (2006).
[47] A. Savin, R. Nesper, S. Wengert, and T. F. Fässler, Angew. Chem., Int. Ed. Engl. **36**, 1808 (1997).
[48] S. M. Selbach, T. Tybell, M.-A. Einarsrud, and T. Grande, Phys. Rev. B **79**, 214113 (2009).
[49] T. E. Westre, P. Kennepohl, J. G. DeWitt, B. Hedman, K. O. Hodgson, and E. I. Solomon, J. Am. Chem. Soc. **119**, 6297 (1997).